This paper is published as part of a PCCP Themed Issue on:
Physical Chemistry of Aerosols

Guest Editors: Ruth Signorell and Allan Bertram (University of British Columbia)

Editorial

Physical Chemistry of Aerosols
Phys. Chem. Chem. Phys., 2009, **DOI:** 10.1039/b916865f

Perspective

Reactions at surfaces in the atmosphere: integration of experiments and theory as necessary (but not necessarily sufficient) for predicting the physical chemistry of aerosols
Barbara J. Finlayson-Pitts, *Phys. Chem. Chem. Phys.*, 2009, **DOI:** 10.1039/b906540g

Papers

Water uptake of clay and desert dust aerosol particles at sub- and supersaturated water vapor conditions
Hanna Herich, Torsten Tritscher, Aldona Wiacek, Martin Gysel, Ernest Weingartner, Ulrike Lohmann, Urs Baltensperger and Daniel J. Cziczo, *Phys. Chem. Chem. Phys.*, 2009, **DOI:** 10.1039/b901585j

Secondary organic aerosol formation from multiphase oxidation of limonene by ozone: mechanistic constraints *via* two-dimensional heteronuclear NMR spectroscopy
Christina S. Maksymiuk, Chakicherla Gayahtri, Roberto R. Gil and Neil M. Donahue, *Phys. Chem. Chem. Phys.*, 2009, **DOI:** 10.1039/b820005j

DRIFTS studies on the photodegradation of tannic acid as a model for HULIS in atmospheric aerosols
Scott Cowen and Hind A. Al-Abadleh, *Phys. Chem. Chem. Phys.*, 2009, **DOI:** 10.1039/b905236d

Infrared spectroscopy of ozone and hydrogen chloride aerosols
Chris Medcraft, Evan G. Robertson, Chris D. Thompson, Sigurd Bauerecker and Don McNaughton, *Phys. Chem. Chem. Phys.*, 2009, **DOI:** 10.1039/b905424n

IR spectroscopy of physical and chemical transformations in cold hydrogen chloride and ammonia aerosols
Evan G. Robertson, Chris Medcraft, Ljiljana Puskar, Rudolf Tuckermann, Chris D. Thompson, Sigurd Bauerecker and Don McNaughton, *Phys. Chem. Chem. Phys.*, 2009, **DOI:** 10.1039/b905425c

Formation of naproxen–polylactic acid nanoparticles from supercritical solutions and their characterization in the aerosol phase
Moritz Gadermann, Simran Kular, Ali H. Al-Marzouqi and Ruth Signorell, *Phys. Chem. Chem. Phys.*, 2009, **DOI:** 10.1039/b901744e

Measurements and simulations of the near-surface composition of evaporating ethanol–water droplets
Christopher J. Homer, Xingmao Jiang, Timothy L. Ward, C. Jeffrey Brinker and Jonathan P. Reid, *Phys. Chem. Chem. Phys.*, 2009, **DOI:** 10.1039/b904070f

Effects of dicarboxylic acid coating on the optical properties of soot
Huaxin Xue, Alexei F. Khalizov, Lin Wang, Jun Zheng and Renyi Zhang, *Phys. Chem. Chem. Phys.*, 2009, **DOI:** 10.1039/b904129j

Spectroscopic evidence for cyclical aggregation and coalescence of molecular aerosol particles
J. P. Devlin, C. A. Yinnon and V. Buch, *Phys. Chem. Chem. Phys.*, 2009, **DOI:** 10.1039/b905018n

Photoenhanced ozone loss on solid pyrene films
Sarah A. Styler, Marcello Brigante, Barbara D'Anna, Christian George and D. J. Donaldson, *Phys. Chem. Chem. Phys.*, 2009, **DOI:** 10.1039/b904180j

Quantifying the reactive uptake of OH by organic aerosols in a continuous flow stirred tank reactor
Dung L. Che, Jared D. Smith, Stephen R. Leone, Musahid Ahmed and Kevin R. Wilson, *Phys. Chem. Chem. Phys.*, 2009, **DOI:** 10.1039/b904418c

Laboratory study of the interaction of HO_2 radicals with the NaCl, NaBr, $MgCl_2 \cdot 6H_2O$ and sea salt surfaces
Ekaterina Loukhovitskaya, Yuri Bedjanian, Igor Morozov and Georges Le Bras, *Phys. Chem. Chem. Phys.*, 2009, **DOI:** 10.1039/b906300e

Kinetics of the heterogeneous reaction of nitric acid with mineral dust particles: an aerosol flowtube study
A. Vlasenko, T. Huthwelker, H. W. Gäggeler and M. Ammann, *Phys. Chem. Chem. Phys.*, 2009, **DOI:** 10.1039/b904290n

Timescale for hygroscopic conversion of calcite mineral particles through heterogeneous reaction with nitric acid
Ryan C. Sullivan, Meagan J. K. Moore, Markus D. Petters, Sonia M. Kreidenweis, Greg C. Roberts and Kimberly A. Prather, *Phys. Chem. Chem. Phys.*, 2009, **DOI:** 10.1039/b904217b

Mid-infrared complex refractive indices for oleic acid and optical properties of model oleic acid/water aerosols
Shannon M. McGinty, Marta K. Kapala and Richard F. Niedziela, *Phys. Chem. Chem. Phys.*, 2009, **DOI:** 10.1039/b905371a

A study of oleic acid and 2,4-DHB acid aerosols using an IR-VUV-ITMS: insights into the strengths and weaknesses of the technique
Sarah J. Hanna, Pedro Campuzano-Jost, Emily A. Simpson, Itamar Burak, Michael W. Blades, John W. Hepburn and Allan K. Bertram, *Phys. Chem. Chem. Phys.*, 2009, **DOI:** 10.1039/b904748d

Deliquescence behaviour and crystallisation of ternary ammonium sulfate/dicarboxylic acid/water aerosols
L. Treuel, S. Pederzani and R. Zellner, *Phys. Chem. Chem. Phys.*, 2009, **DOI:** 10.1039/b905007h

Laboratory chamber studies on the formation of organosulfates from reactive uptake of monoterpene oxides
Yoshiteru Iinuma, Olaf Böge, Ariane Kahnt and Hartmut Herrmann, *Phys. Chem. Chem. Phys.*, 2009, **DOI:** 10.1039/b904025k

Measurement of fragmentation and functionalization pathways in the heterogeneous oxidation of oxidized organic aerosol
Jesse H. Kroll, Jared D. Smith, Dung L. Che, Sean H. Kessler, Douglas R. Worsnop and Kevin R. Wilson, *Phys. Chem. Chem. Phys.*, 2009, **DOI:** 10.1039/b905289e

Using optical landscapes to control, direct and isolate aerosol particles
Jon B. Wills, Jason R. Butler, John Palmer and Jonathan P. Reid, *Phys. Chem. Chem. Phys.*, 2009, **DOI:** 10.1039/b908270k

Reactivity of oleic acid in organic particles: changes in oxidant uptake and reaction stoichiometry with particle oxidation
Amy M. Sage, Emily A. Weitkamp, Allen L. Robinson and Neil M. Donahue, *Phys. Chem. Chem. Phys.*, 2009, **DOI:** 10.1039/b904285g

Surface tension of mixed inorganic and dicarboxylic acid aqueous solutions at 298.15 K and their importance for cloud activation predictions
Alastair Murray Booth, David Owen Topping, Gordon McFiggans and Carl John Percival, *Phys. Chem. Chem. Phys.*, 2009, **DOI:** 10.1039/b906849j

Kinetics of the heterogeneous conversion of 1,4-hydroxycarbonyls to cyclic hemiacetals and dihydrofurans on organic aerosol particles
Yong Bin Lim and Paul J. Ziemann, *Phys. Chem. Chem. Phys.*, 2009, **DOI:** 10.1039/b904333k

Time-resolved molecular characterization of limonene/ozone aerosol using high-resolution electrospray ionization mass spectrometry
Adam P. Bateman, Sergey A. Nizkorodov, Julia Laskin and Alexander Laskin, *Phys. Chem. Chem. Phys.*, 2009, **DOI:** 10.1039/b905288g

Cloud condensation nuclei and ice nucleation activity of hydrophobic and hydrophilic soot particles
Kirsten A. Koehler, Paul J. DeMott, Sonia M. Kreidenweis, Olga B. Popovicheva, Markus D. Petters, Christian M. Carrico, Elena D. Kireeva, Tatiana D. Khokhlova and Natalia K. Shonija, *Phys. Chem. Chem. Phys.*, 2009, **DOI:** 10.1039/b905334b

Effective broadband refractive index retrieval by a white light optical particle counter
J. Michel Flores, Miri Trainic, Stephan Borrmann and Yinon Rudich, *Phys. Chem. Chem. Phys.*, 2009, **DOI:** 10.1039/b905292e

Influence of gas-to-particle partitioning on the hygroscopic and droplet activation behaviour of α-pinene secondary organic aerosol
Zsófia Jurányi, Martin Gysel, Jonathan Duplissy, Ernest Weingartner, Torsten Tritscher, Josef Dommen, Silvia Henning, Markus Ziese, Alexej Kiselev, Frank Stratmann, Ingrid George and Urs Baltensperger, *Phys. Chem. Chem. Phys.*, 2009, **DOI:** 10.1039/b904162a

Reactive uptake studies of NO_3 and N_2O_5 on alkenoic acid, alkanoate, and polyalcohol substrates to probe nighttime aerosol chemistry
Simone Gross, Richard Iannone, Song Xiao and Allan K. Bertram, *Phys. Chem. Chem. Phys.*, 2009, **DOI:** 10.1039/b904741g

Organic nitrate formation in the radical-initiated oxidation of model aerosol particles in the presence of NO_x
Lindsay H. Renbaum and Geoffrey D. Smith, *Phys. Chem. Chem. Phys.*, 2009, **DOI:** 10.1039/b909239k

Dynamics and mass accommodation of HCl molecules on sulfuric acid–water surfaces
P. Behr, U. Scharfenort, K. Ataya and R. Zellner, *Phys. Chem. Chem. Phys.*, 2009, **DOI:** 10.1039/b904629a

Structural stability of electrosprayed proteins: temperature and hydration effects
Erik G. Marklund, Daniel S. D. Larsson, David van der Spoel, Alexandra Patriksson and Carl Caleman, *Phys. Chem. Chem. Phys.*, 2009, **DOI:** 10.1039/b903846a

Tandem ion mobility-mass spectrometry (IMS-MS) study of ion evaporation from ionic liquid-acetonitrile nanodrops
Christopher J. Hogan Jr and Juan Fernández de la Mora, *Phys. Chem. Chem. Phys.*, 2009, **DOI:** 10.1039/b904022f

Homogeneous ice freezing temperatures and ice nucleation rates of aqueous ammonium sulfate and aqueous levoglucosan particles for relevant atmospheric conditions
Daniel Alexander Knopf and Miguel David Lopez, *Phys. Chem. Chem. Phys.*, 2009, **DOI:** 10.1039/b903750k

DRIFTS studies on the photodegradation of tannic acid as a model for HULIS in atmospheric aerosols

Scott Cowen[a] and Hind A. Al-Abadleh*[b]

Received 16th March 2009, Accepted 23rd April 2009
First published as an Advance Article on the web 27th May 2009
DOI: 10.1039/b905236d

Humic like substances (HULIS) are important components of atmospheric aerosols, yet little is known about their photochemical transformation and the role of adsorbed water in this photochemistry. We report herein *in situ* and surface-sensitive spectroscopic studies on (1) the photodegradation of solid tannic acid, (2) structure of adsorbed water before and after photodegradation, and (3) the change in the hydrophilicity of tannic acid as a result of this photochemistry. Tannic acid (TA) was chosen as a synthetic proxy for HULIS because it has a defined molecular structure. Photochemical studies were conducted using diffuse reflectance infrared spectroscopy (DRIFTS) as a function of time (3 h), relative humidity (5–30%) and total irradiance (7, 20, 290 W m^{-2} at 555 nm). Water adsorption isotherm measurements were recorded before and after photodegradation, which provided information on the structure of interfacial water and the thermodynamics of adsorption. The structure of water adsorbed on TA resembles that of water at the interface with polar organic solvents. Difference spectral data collected during irradiation shows loss features in the 1700–1000 cm^{-1} range and growth in carbonyl features that are blue shifted relative to the starting material, suggesting oxidative photodegradation of TA and formation of aryl aldehydes. Under our experimental conditions, we observed no enhancement in water uptake after photodegradation relative to that on unirradiated samples. The implications of our results to the understanding of heterogeneous photochemistry of HULIS and the role of adsorbed water in these reactions are discussed.

1. Introduction

According to the 2007 report by the Intergovernmental Panel on Climate Change, aerosol representation in global circulation models is very uncertain due to their highly complex physico-chemical properties and reactivity that changes with time. One important issue in atmospheric chemistry is the processing and aging of aerosol particles, especially those containing organic matter.[1] Reactions with atmospheric radicals such as NO_x (x = 2, 3), OH and ozone alter aerosols' chemical and physical properties, with direct consequences on the radiative balance of the atmosphere. Oxidation of organics can also occur as a result of near UV-visible light absorption by photosensitizers such as aromatic-containing organics and inorganic NO_2^-/NO_3^-.[2,3] Research in heterogeneous atmospheric chemistry can provide answers to questions related to the *kinetics* and *mechanism* of gas–solid interactions,[1] photochemical reactions in multicomponent aerosols,[3] and the effect of surface chemistry on aerosols physicochemical properties, more specifically, their ability to act as efficient cloud condensation nuclei (CCN).[4]

It is widely recognized that organic-containing aerosols contribute to the change in the radiative balance of the atmosphere through their ability to form CCN and ice nuclei (IN).[1,4] Water uptake by organic-containing aerosols is related to the structure and oxidation state of organic functional groups that, as mentioned earlier, are constantly changing due to aerosols aging. However, due to their complex chemical nature, the aging of humic like substances (HULIS) in aerosols is less-studied than other classes of organic compounds containing fewer reactive functional groups. Atmospheric HULIS are emitted from primary sources such as wind-blown marine, soil and biomass burning, or formed in the atmosphere through condensation and polymerization.[5] HULIS are classified as large multifunctional water soluble organic carbon (WSOC) in aerosols, which makes up to 15–60% of that fraction.[6,7] Duarte *et al.* found from IR and solid state ^{13}C NMR that atmospheric HULIS contain conjugated carbonyl, ethers, aromatic phenols, carboxyl groups, alcohols, oxygenated aliphatic carbons, branched alkyl chains, and a high level of aromaticity and aliphatic content. As a result, most laboratory studies so far have used surrogates for atmospheric HULIS such as humic and fulvic acids from terrestrial and aquatic sources.[8] The hygroscopic growth of these compounds was measured using electrodynamic balance and hygroscopic tandem differential mobility analyzer in their pure form and mixed with inorganic salts[9,10] and insoluble mineral aerosol.[10] These studies found that surrogates for HULIS are efficient CCN, can lower or enhance water uptake when mixed with soluble salts,[9] and can enhance water adsorption when coating insoluble calcite particles.[10]

[a] *Department of Chemistry, University of Guelph, Guelph, Ontario, Canada*
[b] *Department of Chemistry, Wilfrid Laurier University, Waterloo, Ontario, Canada*

There are few studies on the heterogeneous chemistry of atmospheric HULIS with atmospheric radicals, their photodecomposition by radicals generated from the absorption of near UV-visible light, and the role of adsorbed water in this photochemistry.[1,8,11–13] Such studies are important in understanding structural changes to HULIS as a result of photochemical reactions, and their impact on the hygroscopic properties of HULIS. For example, atmospheric HULIS extracted from wood burning and urban pollution atmospheric particles were found to enhance the oxidation of pyrene and phenol in the aqueous phase by promoting a dark Fenton process.[11] Fast photosensitised formation of HONO was observed in the reaction of NO_2 on humic acids under humid conditions.[12,13] It was proposed from gas phase uptake experiments that activation of reductive centres (A_{red}) within humic acid by light can result in reaction with adsorbed NO_2 species to form HONO leaving behind oxidized humic acid. Clearly, more systematic studies are needed that investigate the role of adsorbed water in these surface reactions, the mechanism that accounts for the photoenhanced loss of gases such as NO_2, and formation of surface products such as organonitrogen and more oxygenated species that can impact the hygroscopic nature of HULIS.

Motivated by the aforementioned studies and the limited number of experimental works on the heterogeneous chemistry of atmospheric HULIS, we report herein *in situ* and surface-sensitive spectroscopic studies on the photodegradation of solid tannic acid as a function of time, relative humidity and total irradiance, the structure of water adsorbed on tannic acid before and after photodegradation, and the change in the hydrophilicity of tannic acid as a result of this photochemistry. Tannic acid (TA, 1,2,3,4,6-pentagalloyl-*O*-glucose, $C_{76}H_{52}O_{46}$) was chosen as a synthetic proxy for atmospheric HULIS instead of humic or fulvic acids[8] for the following reasons. TA has a defined molecular structure (Fig. 1A) with fewer functional groups compared to terrestrial and aquatic humic substances. The defined molecular structure is helpful in understanding the photodegradation mechanism of TA and properties of interfacial water studied herein. It is a multifunctional macromolecule that contains a sugar ring bearing polyphenols connected by ester groups. TA has H : C and O : C ratios of 0.68 and 0.61, respectively, which makes it a more-oxygenated HULIS surrogate with a higher degree of unsaturation and weaker acidity than aquatic humic substances.[14] Its structure also resembles polyaromatic hydrocarbons (PAHs) aged by oxidation due to reaction with O_3,[15–17] and urban-influenced aerosols containing high concentrations of ester, lactone and PAH.[18] Our studies were conducted using diffuse reflectance infrared spectroscopy (DRIFTS), which has proven to be a powerful tool for studying the heterogeneous chemistry of model components in aerosols, *in situ* and in real time.[19] Photodegradation experiments were conducted as a function of time (3 h) and relative humidity (5–30%) using near UV-visible light (300–800 nm) from a Xe lamp with total irradiance of 7, 20 and 290 W m^{-2} (at 555 nm). Water adsorption isotherm measurements were recorded before and after photodegradation, which provided information on the structure of interfacial water and the thermodynamics of adsorption.

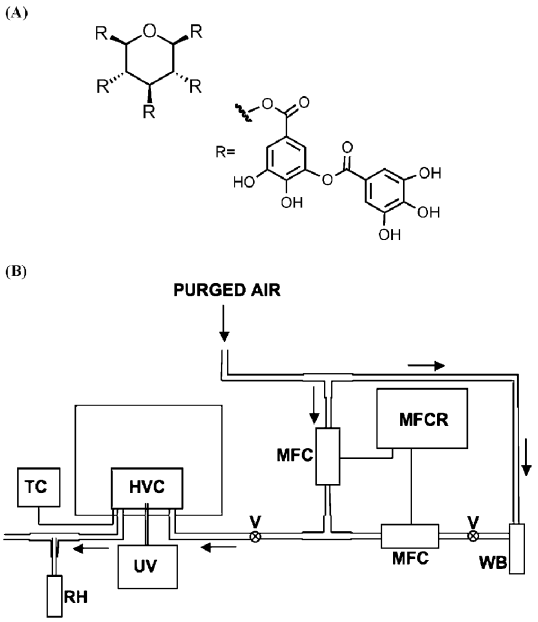

Fig. 1 (A) Structure of TA.[22,45] (B) Schematic of the DRIFTS apparatus and the gas handling system: TC is a thermocouple, HVC is the DRIFTS HVC reactor chamber, RH is a relative humidity gauge, UV is the ultraviolet-visible light source, V are ball valves, MFC are mass flow controllers, MFCR is the readout for the mass flow controllers and WB is the water bubbler.

2. Experimental

DRIFTS spectra were collected using a Praying Mantis diffuse reflectance accessory (Harrick, DRK-4-NI8) with a high temperature stainless steel reaction chamber treated with a special SilcoSteel-CR coating. The reaction chamber contains a sample cup (depth 3 mm, dia. 6 mm) and was covered with a treated stainless steel cover equipped with two ZnSe optical windows and a central quartz viewing window. For photochemical experiments, two light sources were used: 35 W Xe lamp (300–800 nm, Mikropack HPX-2000), and 150 W Xe lamp (solar simulator, Newport Corp.). A fiber optic cable (Ocean Optics) was connected to the 35 W Xe lamp and directed at the sample through the viewing quartz window, whereas a fiber bundle focusing assembly connected to a liquid light guide (Newport Corp.) was used to deliver light from the 150 W solar simulator to the sample. Total irradiance between 300–800 nm was measured at the sample surface using a digital lux meter. Experiments were performed using 4700 lux (*ca.* 7 W m^{-2}), 13 400 lux (*ca.* 20 W m^{-2}), and 198 000 (*ca.* 290 W m^{-2}) at 555 nm.

The DRIFTS accessory was installed in a Nicolet 8700 FTIR spectrometer (Thermo Instruments) equipped with a purge gas generator and a liquid N_2-cooled MCT detector. All spectra were collected at 4 cm^{-1} resolution by averaging 300 scans/spectrum. The temperature of the reaction chamber was monitored by thermocouples connected to a temperature controller (Harrick ATC-024-1). The chamber has two ports for flow mode experiments and was connected to the gas handling system as shown in Fig. 1B, which was constructed from PFA tubing and fittings (Swagelok). Purged air (Parker Balston Analytical Gas Systems FT-IR Purge Gas

Generator 75–52) is separated into two streams: one enters a water bubbler (Dimaglass) containing 18.2 MΩ water (Millipore Milli-Q Plus) to generate humid air, and the second stream remains dry. Using mass flow controllers (MKS Type 1479A MFC) and a readout (MKS Type 247D), the flow rates of the humid and dry air were altered to vary the relative humidity (RH) of mixed air entering the sample chamber. A relative humidity sensor (Vaisala HUMICAP HM70) was used to monitor the relative humidity of air exiting the chamber.

For DRIFTS measurements to be reproducible, the sample must be as homogeneous and well-packed as possible. Commercially available TA (Alfa Aesar, 53.2% C, 3.3% H, 43.3% O by elemental analysis) was ground using a wig-L-bug 6 times for 1 min each. This process resulted in particle size of 5 ± 2 μm, and BET surface area 3.5 ± 0.3 m^2 g^{-1} using N_2 as an adsorbent. Since TA displays high absorbance in the IR region, the sample was diluted with a relatively efficient scattering material that is non-hygroscopic and unreactive. Diamond powder (used as is, Lands Superabrasives LST600T, particle size 5 ± 2 μm, BET area 0.89 ± 0.02 m^2 g^{-1}) was found to fulfil these conditions. Fig. 2A shows scanning electron microscopy images of diamond powder (left) and ground TA (right). Tannic acid was mixed with diamond powder in ratios of 1–10% wt/wt, respectively, and shaken for 1 min using the wig-L-bug without using the grinding ball. About 0.23 g of the mixture filled the sample cup in the reaction chamber, and a 4 kg press was used for 10 min for reproducible packing. Fig. 2B shows a DRIFTS absorbance spectrum of 6% (wt/wt) of TA at <1% RH and the assignment of the bands is discussed in the next section. Single beam spectra were collected for diamond powder as a reference and mixed TA/diamond samples as a function of concentration.

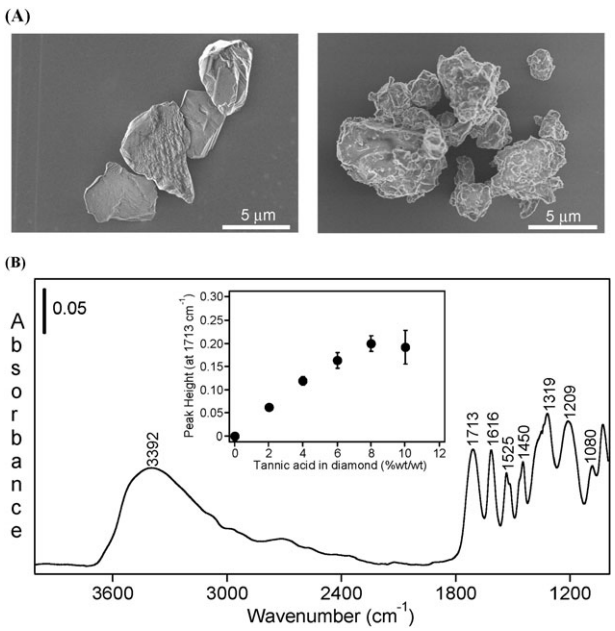

Fig. 2 (A) SEM images of 6 micron diamond (left), and tannic acid (right). (B) DRIFTS absorbance spectrum of 6% (wt/wt) tannic acid. The inset is the calibration curve of DRIFTS absorbance at 1713 cm^{-1} *versus* wt% of tannic acid in diamond.

According to Sirita *et al.*,[20] transformation of DRIFTS single beam spectra to absorbance (instead of Kubella–Munk function) is proportional to concentration if $I_{sample}/I_{referene}$ is higher than *ca.* 60% at a given wavenumber. For our case, we found that $I_{(TA/diamond)}/I_{diamond}$ is about 58% at 1713 cm^{-1} for a 6% TA (wt/wt). Hence, the absorbance at 1713 cm^{-1} was used to construct a calibration curve as a function of TA wt% in diamond (inset of Fig. 2B). The linearity of this calibration curve using absorbance conversion of single beam DRIFTS spectra instead of the Kubella–Munk transformation suggests that the scattering coefficient is constant over the TA concentration range used, which also indicates a reproducible packing of our samples.[21]

Two types of experiments were completed: water adsorption/desorption isotherm experiments on unirradiated and irradiated TA samples as a function of RH, and photochemical experiments using near UV-visible light at 5, 20 and 30% RH for 3 h. For isotherm experiments, the TA sample was packed and exposed to dry air overnight. A scan is taken of the dry sample and used as the reference for spectra collected as a function of RH. When the desired relative humidity is reached after mixing dry and humid air, the sample is allowed to equilibrate for 15 min with the gas phase before a spectrum is taken. Longer equilibrium times did not result in significant increases in the absorbance assigned to adsorbed water at 1645 cm^{-1}. Although the IR pathlength inside the DRIFTS accessory is relatively short, spectral features assigned to gas phase water remained visible in the spectra collected using TA as a function of RH. Spectral subtraction of these features was possible by using DRIFTS absorbance spectra of gas phase water collected using a reflective mirror instead of the reaction chamber inside the Praying Mantis. For photochemical experiments, the TA sample was allowed to equilibrate at the desired RH for 20 min before turning the lamp on. A "dark" spectrum was then collected and used as the reference for spectra collected after irradiation as a function of time (3 h) and constant RH. The RH sensor showed that RH does not vary more than 5%, and the sample temperature did not increase more than 2 °C due to local heating. Water uptake on TA samples after irradiation was measured after drying overnight according to the aforementioned procedure.

3. Results and discussion

3.1 Infrared characterization of solid tannic acid

The DRIFTS absorbance spectrum of TA (6% wt/wt) is shown in Fig. 2B, and the assignment of the observed bands is summarized in Table 1. The absorbance spectrum is in excellent agreement with that collected by Jastrzebska *et al.* from a KBr pellet of TA in the transmission mode.[22] The assignment was based on the chemical structure of TA shown in Fig. 1A and was compared to the IR bands observed for atmospheric HULIS.[5] Bands observed in the spectral range 1800–1000 cm^{-1} are more defined than those observed for hydrophobic acids of WSOC extracted from atmospheric aerosols and Suwannee River humic and fulvic acids.[14] This region contains bands assigned to the stretching vibration (ν)

Table 1 Assignment of infrared bands observed in the DRIFTS absorbance spectrum of TA and difference spectra during water adsorption and photodegradation

Vibrational mode	Wavenumber/cm^{-1} TA (as is, dry)	TA (dissolution due to water adsorption)	TA (during photodegradation)	Previous studies (FTIR)	References
ν(C–O–C) of carbohydrate moieties and ethers	1080	1045 (+ve)	1038 (−ve)	1036	32
				1040	31
				1080	14 and 32
ν(C–O) of secondary alcohol			1072 (+ve)	1085–1050	46
			1140, 1145 (+ve)	1205–1124	31
				1120	
ν[C–O(C═O)]		1161 (−ve)		1190–1141	46
	1209	1298 (−ve)	1205, 1215 (−ve)	1200	14
				1310–1250	46
δ(–CH) aromatic rings		1252 (+ve)		1275–1200	
aromatic ring breathing vibrations	1319		1333 (−ve)	1332	14
δ(C–O–H) or δ(–OH) interaction with ν(C–O)	—	1350 (+ve)		1335–1375	24
ν(C–C) of aromatic rings	1450	1454 (+ve)	1448, 1454 (−ve)	1450	14
	1525		1539, 1541 (−ve)	1518	14 and 32
	1616		1614, 1620 (−ve)	1600–1660	14 and 32
				1640	31
ν(C═O) conjugated	1713	1743 (−ve)	1703 (−ve)	1714	31
Unconjugated			1753–1761 (+ve)	1720	14
				1743	31
ν(OH) in phenol	3392			3400	14

of C–O at 1080 and 1209 cm^{-1}, aromatic ring breathing vibrations and C–H in-plane deformation at 1319 cm^{-1}, respectively, stretching vibration of aromatic C–C bonds at 1450, 1525 and 1616 cm^{-1}, and stretching vibration of unconjugated C═O groups in ester links [–C(O)O–] between polyphenol substituents at 1713 cm^{-1}. The stretching vibration of OH phenolic groups exhibits a broad feature centered at 3392 cm^{-1}. Other differences between the IR spectra of TA and those of atmospheric HULIS include the absence of features in the spectral range 3000–2850 cm^{-1} assigned to the C–H stretching vibration of methyl (–CH_3) and methylene (–CH_2–) groups of aliphatic chains, and the lower intensity of the ν(C═O) relative to other neighboring bands.[5,14] The latter observation may be due to the absence of carboxyl groups identified in HULIS.

3.2 Structure of water adsorbed on solid tannic acid

Fig. 3 shows difference absorbance spectra of water adsorption as a function of increasing RH on (a) unirradiated TA, and (b) after photodegradation of TA using 20 W m^{-2} near UV-visible light at 20% RH. Single beam spectra collected as a function of RH were referenced to the spectrum of dry TA followed by subtracting absorptions due to gas phase water. These difference absorbance spectra show that increasing RH results in increasing the intensity of spectral features assigned to adsorbed water, which are the bending mode $\delta(H_2O)$ at 1645 cm^{-1} and the stretching vibration of hydrogen bonded OH groups ν(OH) between 3700 and 2500 cm^{-1}. The bending mode was used to quantify the relative amounts of adsorbed water on the surface of TA (*vide infra*). The spectral region containing this mode also shows positive (1454, 1350, 1252 and 1045 cm^{-1}), and negative features (1743, 1298 and 1161 cm^{-1}) that become more pronounced with increasing RH (see Table 1 for assignments). Changes in the spectral region between 1800–1000 cm^{-1} are rarely analyzed for water adsorption on organic surfaces (see references in ref. 23). In addition to $\delta(H_2O)$, this region contains most of the

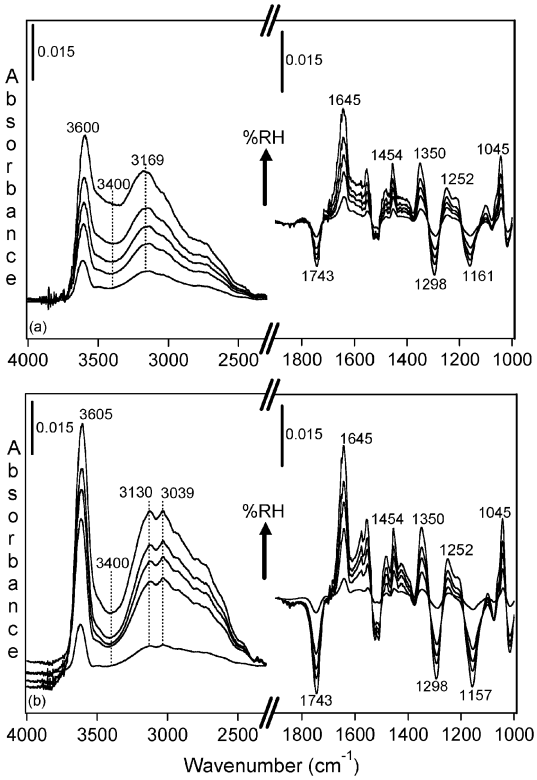

Fig. 3 Absorbance spectra of water adsorbed on tannic acid as a function of increasing RH (a) unirradiated (5.5, 22, 40, 60, and 84% RH), and (b) after irradiation for 3 h at 20% RH (Xe lamp, 20 W m^{-2}) at 2, 23, 40, 58, and 81% RH. Reference spectrum is tannic acid dried by flowing <1% RH air overnight.

fundamental vibrational modes of organic functional groups present in organic-containing aerosols. Since spectra shown in Fig. 3 were obtained by using dry TA as the reference, trends observed in the spectral region below 1800 cm^{-1} suggest changes to the phase of the starting material with increasing RH. As explained below, our studies show that water adsorption on TA leads to the dissolution of TA at the interface or the formation of TA-hydrates.

The formation of TA-hydrates is likely to occur in a manner similar to that observed for glucose, fructose[24] and sucrose[25] using attenuated total internal reflectance Fourier transform infrared spectroscopy (ATR-FTIR). The analysis of the IR spectra of these carbohydrate units as a function of concentration in liquid water suggested the formation of penta- and dihydrates for glucose and sucrose, and penta- and monohydrate for fructose. Band positions and intensities of features assigned to ν(C–O) in the 1100–1000 cm^{-1} spectral range are most sensitive to these hydrates. For instance, the spectrum of glucose dihydrate shows bands at 1076 and 1027 cm^{-1} that increase in frequency to 1081 and 1034 cm^{-1} upon the formation of glucose pentahydrate. However, this blue shift is accompanied by a reduction in the intensity of the higher frequency band and an increase in the intensity of the low frequency band. Similar observations were found for fructose, and it was related to a reduction in the strength or number of hydrogen bonds accepted by the oxygen atom.[24] By analogy, the spectra in Fig. 3a and b suggests that C–O bonds in TA (before and after photodegradation) are involved in hydrogen bonding with interfacial water, resulting in the growth of spectral features at 1045 cm^{-1} assigned to ν(C–O) in hydrated TA. Consistent with this interpretation is the growth of the feature at 1350 cm^{-1} assigned to δ(C–O–H) or arising from the interaction of δ(–OH) interaction with ν(C–O). Other positive features include those at 1252 and 1454 cm^{-1} related to δ(–CH) and ν(C–C) or aromatic rings in the TA-hydrate species. Moreover, loss features at 1743, 1298, and 1161 cm^{-1} are associated with hydrogen bonding acceptors such as C–O(C═O) and suggest weakening in these bonds relative to the same groups present in dry TA. This observation along with the intensity increase of positive features with increasing RH further support the presence of dissolved TA with increasing amounts of adsorbed water due to an increase in the solvent to solute ratio. As expected, control DRIFTS experiments for water adsorption on diamond powder (water insoluble) show the absence of loss and growth features in the spectral range between 1800–1000 cm^{-1}, except for $\delta(H_2O)$.

Moreover, analysis of the spectral region between 3700 and 2500 cm^{-1} provides information on the structure of adsorbed water on TA. Fig. 3a for unirradiated TA shows that this region contains a broad feature centered at 3169 cm^{-1} assigned to ν(OH) of hydrogen bonded water, and a sharp feature centered at 3600 cm^{-1} assigned to ν(OH) of dangling or "free" OH groups. Both of these features increase in intensity with increasing RH. Spectra for water adsorption on photodegraded TA shown in Fig. 3b contain a more structured broad feature with components at 3130 and 3039 cm^{-1}, and a sharp feature at 3605 cm^{-1}. The data does not rule out the existence of a relatively small intensity component at $\sim$3400 cm^{-1} that also increases in intensity with increasing RH. Most infrared spectroscopic studies on water adsorption from the gas phase are conducted on flat surfaces terminated with organic functional groups, and were recently reviewed by Moussa *et al.*[23] and Asay *et al.*[26] In general, low-frequency components of ν(OH) of adsorbed water on organic surfaces are analyzed relative to that of liquid water at $\sim$3400 cm^{-1} and ice at $\sim$3200 cm^{-1}. It was found from experimental data and molecular dynamic simulations of water clusters on hydrophobic organic monoalyers that relative intensities of the 3200/3400 cm^{-1} components correlate with the number of hydrogen bonds among water molecules.[23] Water molecules in contact with organic monolayers at low RH have fewer hydrogen bonds and give rise to spectral components at 3200 cm^{-1}, whereas molecules in the interior of water clusters have 3 and 4 hydrogen bonds similar to that of bulk water.

Our spectroscopic results shown in Fig. 3 are the first to be recorded on a solid porous multifunctional organic material. It is interesting to note that features observed in the spectral region between 3700 and 2500 cm^{-1} in Fig. 3 are similar to those observed in the sum frequency generation (SFG) spectra of water molecules at the vapor/water and organic/water interfaces.[27,28] The SFG spectra of water at these interfaces show broad features extending from 3500 to 3000 cm^{-1} with a maximum around 3480 cm^{-1} for the vapor/water interface that blue shifts to $\sim$3500 for CCl_4/water interface. This broad feature was assigned to water molecules involved in strong hydrogen bonding with nearby water molecules at the interface.[27] Recently, Nichols *et al.*[29] studied the reaction of a benzophenone-catechol mixture with NO_2 under dark conditions at 20% RH using ATR-FTIR, and noticed an increase in the absorption of a broad feature between 2000–3000 cm^{-1} with reaction time. This structured feature, with resolved components at 3100 and 2900 cm^{-1}, was assigned to ν(OH) of strongly hydrogen bonded adsorbed water on the solid phase of more hygroscopic reaction products (mostly 4-nitrobenzene-1,2-diol). Based on these studies, and provided with the chemical structure of water–soluble TA, our data suggests the formation of strong hydrogen bonding network in TA-hydrates arising from TA–water or water–water interactions at the interface, which dominate at low and high RH. This network could be due to the formation of fewer than 4 hydrogen bonds unlike in bulk water. The growth of the component at 3400 cm^{-1} suggests either water condensation in the pores of TA or the formation of a more "liquid-like" hydrogen bonding network among adsorbed water molecules. Additionally, surface photodegradation products of TA seem to influence the hydrogen bonding network in adsorbed water, evident by the red shift of the broad feature maximum by about 39 cm^{-1} and the increase in the intensity of a lower frequency component at 3039 cm^{-1}. This observation suggests that hydrogen bonding of water to oxidized photodegradation products of TA is similar to that of water to –COOH-terminated self-assembled monolayers,[23] where the formation of one or two strong hydrogen bonds has the highest probability.

Moreover, analysis of the sharp feature assigned to ν(OH) of dangling or "free" OH groups (centered at *ca.* 3600 cm^{-1}) further supports the above discussion. High frequency features

have been observed in the SFG spectra of interfacial water molecules near 3700 cm^{-1}, which are referred to as the "free OH" mode of highly oriented water molecules.[27] This feature is narrow and centered at 3705 cm^{-1} for vapor/water that is red shifted to 3674 cm^{-1} for alkanes/water, 3669 cm^{-1} for CCl_4/water and 3650 cm^{-1} for $CDCl_3$/water interfaces. This sharp feature was used as an indicator for the presence of water–organic interactions and the relative strength of this interaction: the lower the frequency of "free" ν(OH), the stronger the water–organic interaction. Hence, the aforementioned trend observed in SFG studies is indicative of a weaker alkane–water than CCl_4–water interaction, and that the strongest interaction is observed for water at the $CDCl_3$/water interface due to its higher polarity. It was concluded from these studies, which were complemented by molecular dynamic calculations, that these weak interactions drive a molecular ordering behavior that extends well into the organic phase.[27] By analogy, our results suggest that due to the high polarity of the oxygenated functional groups in TA, water–water and/or TA–water hydrogen bonding interactions are stronger than water–water interactions at the vapor/water interface. The presence of the feature at *ca.* 3600 cm^{-1} suggests substantial orientation of water molecules near TA in a fashion similar to that observed for the above organic interfaces.

3.3 Photodegradation of solid tannic acid as a function of time, RH and total irradiance

We investigated the photodegradation of TA as a function of time (3 h) and relative humidity (5–30%) using near UV-visible light (300–800 nm) from a Xe lamp with total irradiance of 7, 20 and 290 W m^{-2} (at 555 nm). Panel A of Fig. 4 shows DRIFTS absorbance spectra in the range 1900–900 cm^{-1} recorded as a function of time at RH values of 5, 20 and 30% using 7 W m^{-2} irradiance (left), and at 20 and 30% using 20 W m^{-2} irradiance (right). These RH values result in surface water coverage below and above a monolayer as determined from the BET adsorption model (*vide infra*). The reference single beam spectrum used to generate these absorbance spectra is that recorded for TA at equilibrium with the desired RH for at least 20 min before turning the lamp on. These spectra clearly show negative and positive features indicating changes in the bonding arrangements of functional groups relative to the starting material as a result of irradiation. The assignment of these spectral features is given in Table 1, which is in excellent agreement with previous spectroscopic studies on the photodegradation of aquatic humic substances.[30–32] Negative features are associated with the carbohydrate moiety (1038 cm^{-1}), aromatic rings (1333 and 1446–1620 cm^{-1}), and ester linkages (*ca.* 1210 and 1703 cm^{-1}) of TA suggesting either bonds breakage or changes in the nature of substituents as a result of photon absorption. The positive spectral features suggest the formation of products containing aliphatic secondary alcohol groups (1072, 1140 and 1145 cm^{-1}) and unconjugated carbonyl groups (1753–1761 cm^{-1}) such as aromatic aldehydes.[31]

The growth in the carbonyl spectral feature (1753–1761 cm^{-1}) has minimum contributions from other features, and hence,

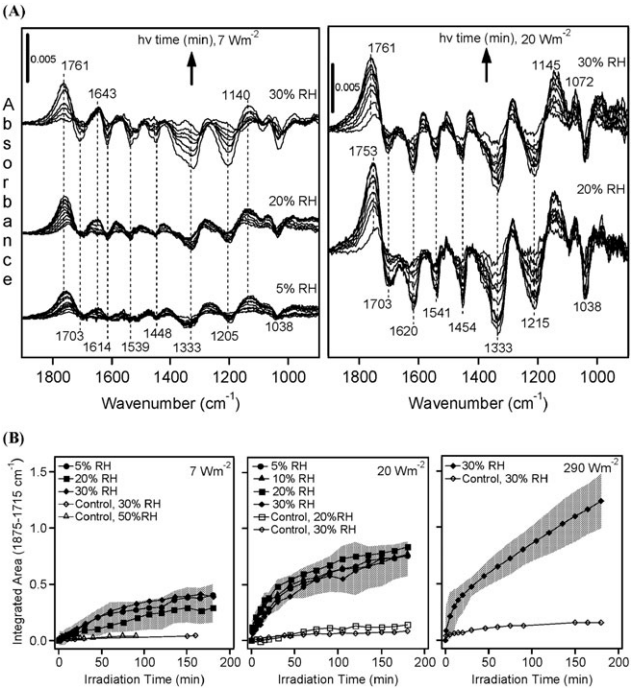

Fig. 4 Photodegradation of tannic acid as a function of irradiation time (max. 3 h). Panel (A): absorbance spectra recorded as a function of relative humidity while irradiation with 7 W m^{-2} (left) and 20 W m^{-2} (right) total irradiance. Panel (B): Integrated area of the band assigned to unconjugated C=O in the spectral range 1875–1715 cm^{-1} as a function of irradiation time and relative humidity while irradiation with 7 W m^{-2} (left), 20 W m^{-2} (center), and 290 W m^{-2} (right). Control experiments are obtained from irradiating diamond only at a given relative humidity. The shaded area shows the uncertainty in the integrated area values.

the integrated area of this band was used to generate kinetic curves as a function of time. These curves are shown in panel B of Fig. 4, which quantify the temporal extent of the oxidative photodegradtion of TA as a function of RH and total irradiance. Each data point is the average value from 2–3 DRIFTS experiments on different TA samples under the same experimental conditions. The uncertainty in these values is represented by the shaded area. Data points from control experiments (no TA present) are also shown, which further supports the above assignment to be due to oxidative photodegradation of TA. Analysis of the data shown in panel B of Fig. 4 shows that there are two kinetic regimes within the 3 h irradiation time. Initial growth kinetics quantified through the determination of slopes from the data normalized to the integrated area at about 20 min show that initial rates are about 0.05 for total irradiance of 7 and 20 W m^{-2}, and 0.08 min^{-1} for 290 W m^{-2}, independent of RH in the range investigated. The extent of photodegradation for times longer than 20 min continues at relatively slower rates with no signs of saturation. The fast kinetic regime is due to the photodegradation of TA-hydrates already formed at a given RH before turning the light on. The slower kinetics regime suggests that longer irradiation times allow for further dissolution of TA to happen, followed by photodegradation of newly dissolved species. Our data suggests that both of these regimes depend on the intensity of irradiation used.

The spectral data on the structure of water on TA suggests the formation of TA-hydrate clusters through interactions with hydrogen bond acceptor groups. The water content of these clusters at a given RH limits the amount of TA dissolved (or TA-hydrates). The fact that we observe (1) a kinetic behavior that is independent of RH in the range 5–30%, and (2) no signs for saturation with irradiation times as long as 3 h at a given RH suggest that the contact area of water with dry TA at these RH values is the same, which increases as TA photodegrades allowing for further dissolution to occur. As discussed by Moussa *et al.*,[23] the contact area of water is sensitive to the hydrophilic nature of solid organic surfaces. Hence, under our experimental conditions (RH = 5–30%), it is very likely that the contact area of water clusters forming at the RH values studied increases as oxidative photodegradation takes place (forming more hydrophilic products), and thus increasing dissolution and concentration of TA-hydrates that undergo photodegradation. Hence, the slower kinetics regime shown in panel B of Fig. 4 is a composite of dissolution and photodegradation rates giving rise to slower kinetics than initial photodegradation. The atmospheric implications of these findings are discussed below.

There are a number of excellent reviews on the mechanism of photochemical reactions involving humic substances in atmospheric aerosols and aquatic systems.[3,33–36] Briefly, light absorption by dissolved organic matter (DOM) in the presence of oxygen leads to the formation of OH radicals and H_2O_2, which are efficient oxidizers of organic matter. In light of this known photochemistry, and the spectral analysis discussed above, a proposed mechanism for the oxidative photo degradation of TA is shown in Fig. 5. Light absorption by TA leads to a ring opening of the carbohydrate moiety, followed by hydrogen abstraction, leading to the formation of a secondary alcohol. In addition, upon light absorption by the polyphenol substituents of TA, breakage of the ester linkages forms three organic radicals. These radicals are quenched through a series of hydrogen abstractions and OH additions, eventually releasing CO_2 into the gas phase and forming 1,2,3-benzenetriol and 2,3,4-trihydroxybenzaldehyde. This mechanism is consistent with that suggested by Mang *et al.*[37] for the aging of secondary organic aerosol (SOA), where photolysis of carbonyl groups in monoterpene SOA resulted in the formation of CO and other low molecular weight aldehydes. The resonance structure of the latter product breaks the aromaticity of the ring forming a quinone. The formation of the aryl aldehyde is responsible for the high frequency ν(C=O) in the range 1753–1761 cm^{-1}. To summarize, TA undergoes oxidative photodegradation upon irradiation with near UV-visible light of intensity as low as 7 W m^{-2} under humid conditions. The initial kinetics of this photochemistry depends on the total irradiance, appears to be fast within the first 60 min, independent of RH and results in the formation of lower molecular weight polyphenols that are more hydrophilic than unirradiated TA. The impact of this photochemistry on water uptake by TA is discussed in the next section.

3.4 Water uptake on tannic acid before and after photodegradation

Fig. 3 shows DRIFTS absorbance spectra collected for water adsorption on TA before and after photodegradation.

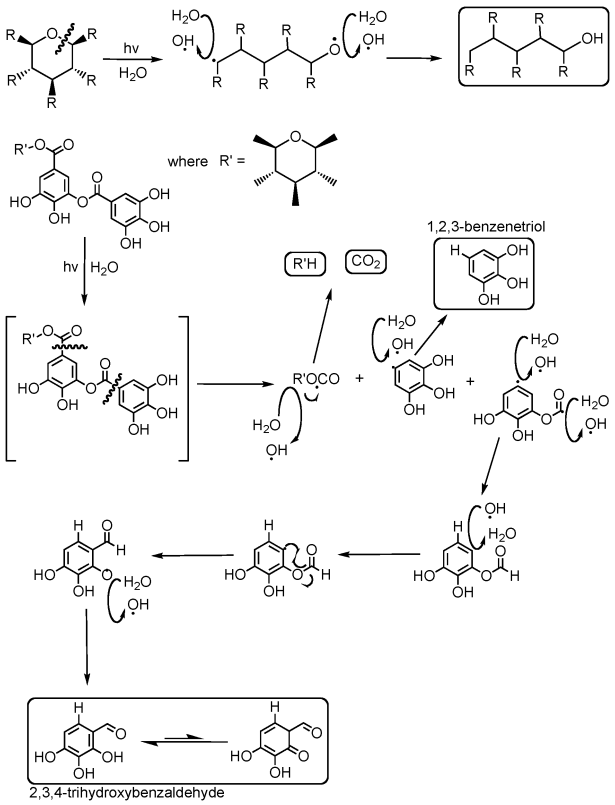

Fig. 5 Proposed mechanism of tannic acid photodegradation.

The integrated area of the bending mode of water, $\tilde{A}[\delta(H_2O)]$, was used to quantify the amount of water adsorbed as a function of increasing and decreasing RH. The adsorption isotherms on unirradiated and irradiated TA samples are shown in Fig. 6A. The data indicates continuous water uptake with no phase transitions, which is consistent with the studies by Chan *et al.*,[9] who found that neither deliquescence nor efflorescence occur on natural fulvic acids. Instead, continous water uptake is seen with increasing RH and residual water is retained even at very low RH (<10%). This data clearly shows a Type II adsorption isotherm indicative of multilayer adsorption that can be modeled using the 2-parameter BET adsorption model, which assumes the formation of infinite number of layers. This model was used to fit the absolute values of $\tilde{A}[\delta(H_2O)]$ as a function of increasing RH, which resulted in a good fit up to 50% RH. This observation suggested that adsorption of water on TA is limited to a given number of layers, which is a behavior observed for water adsorption on porous metal oxides.[38] Goodman *et al.*[38] used a modified BET model with a third adjustable parameter, *n*, that limits the number of adsorbed layer at high RH values and found that *n* values ranged from 3–10. This parameter is related to the pore size and properties of the adsorbent.[38] The modified BET model was used to fit the experimental data shown in Fig. 6 according to the procedure described in detail by Goodman *et al.*[38] The best fit parameters are listed in Table 2, where it can be clearly seen that the first layer of adsorbed water forms around 20% RH, and that despite photodegradation, the enthalpy of water adsorption is similar on both samples. The data also suggests

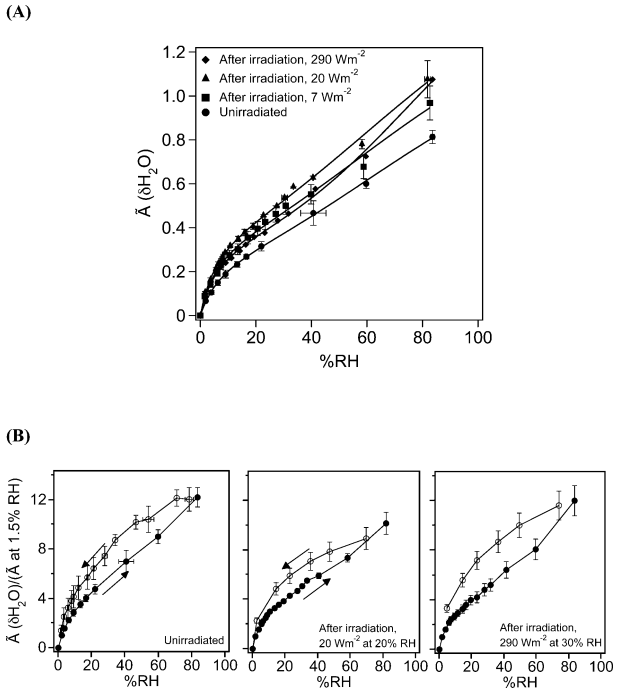

Fig. 6 (A) Water adsorption isotherms on tannic acid samples at 298 K before and after irradiation with near UV-visible light of 7 and 20 W m^{-2} total irradiance at 20% RH, and 290 W m^{-2} at 30% RH. The lines through the data are the best fit using the modified 3-parameter BET adsorption model.[38] Fitting parameters are listed in Table 2. (B) Relative amounts of adsorbed water calculated by normalizing the data shown in (A) to the integrated area of $\delta(H_2O)$ at $\sim$1.6% RH. Solid and empty markers represent data collected at increasing and decreasing RH, respectively.

that under our experimental conditions of total irradiance and %RH, water uptake on unirradiated TA is similar to that after irradiation with near UV-visible light.

The fact that a monolayer of adsorbed water is predicted to occur at *ca.* 20% RH for all samples studied suggests no enhanced uptake of water on photodegraded TA. This conclusion does not quite agree with the isotherm data shown in Fig. 6A, which at first glance, suggests the opposite. To quantify the relative amount of water adsorbed as a function of increasing and decreasing RH, $\tilde{A}[\delta(H_2O)]$ was normalized to that at $\sim$1.6% RH for each data set shown in Fig. 6A. This relative humidity was chosen as a reference point independent of the BET isotherm analysis, and it represents the amount of water at the lowest measurable RH value on unirradiated and irradiated TA samples that were dried overnight by air flow of $<$1% RH. The results are presented in Fig. 6B and clearly show similar water uptake on the TA samples studied herein with no enhancement due to photodegradation. This observation is consistent with the findings of Moussa *et al.*[23] and McIntire *et al.*[39] who reported no increase in the water uptake on oxidized self assembled monolayers. However, the TA system is different from monolayers anchored to silica or gold substrates in that it is photoreactive and water soluble. Our studies show that the extent of TA photodegradation is dependent on total irradiance of the near UV-visible light used, where using an intense light source (290 W m^{-2}) resulted in continuous formation of more oxidized products evident by the slow and near linear growth of the band assigned to carbonyl functional group for as long as 3 h. As discussed above, this observation suggests an increase in the contact area of water clusters with photodegraded TA causing further dissolution of TA with time followed by photodegradation in the RH range investigated (5–30%). This RH range, however, is below and slightly above a monolayer of adsorbed water as determined by the modified BET isotherm. While there is evidence for the formation of TA-hydrates at these RH values (*vide supra*), it is likely that the solvent/solute ratio in these studies was not high enough to cause extensive photodegradation of TA in a manner similar to that in solution. The possibility of whether an enhancement in water uptake will occur on TA photodegraded at RH values above a monolayer and using an intense light source (290 W m^{-2}) is currently being investigated in our lab.

Moreover, the desorption data clearly shows hysteresis when compared to the adsorption data. Both adsorption and desorption data were collected after 15–20 min equilibrium at a given RH. Spectra collected at longer equilibrium times (up to 1 h) show only a change of 7% in the surface concentration of water represented by $\tilde{A}[\delta(H_2O)]$, which is within the uncertainties of our measurements. Hence, we concluded that the diffusion of water from the bulk of the sample to the near surface region probed by the IR beam occurs on the same time-scale allowed for equilibrium to be established with the gas phase. The hysteresis suggests slower desorption kinetics of water from TA and its photodegradation products, which correlates well with our structural analysis of adsorbed water layers suggesting strong TA–water and water–water interactions (*vide supra*). Our results are consistent with hygroscopic growth experiments on natural fulvic acids[40] and model HULIS[9] using electrodynamic balance and hygroscopic tandem differential mobility analyzer that show

Table 2 Best fit parameters of the modified BET adsorption model to the experimental data of water adsorption on TA

Sample	n	$\tilde{A}[\delta(H_2O)]_{ML}$	c	$-\Delta H^{\circ}_{ads}$/kJ mol^{-1}
Unirradiated TA	5.0(0.2)	0.31(0.01)	12(1)	50(4)
After irradiation, 7 W m^{-2}	4.8(0.3)	0.38(0.01)	16(2)	51(6)
After irradiation, 20 W m^{-2}	4.9(0.2)	0.42(0.01)	16(1)	51(3)
After irradiation, 290 W m^{-2}	6.2(0.2)	0.35(0.01)	17(1)	51(3)

Note: The best fit parameters are defined in ref. 38 as following: n: adjustable fitting parameter that limit the number of adsorbed layers at high RH, $\tilde{A}[\delta(H_2O)]_{ML}$: the integrated area of the bending mode of water at a monolayer surface coverage, c: is the temperature-dependent constant related to the enthalpy of first layer adsorption, ΔH°_{ads}, and that of higher layers, ΔH°_{cond}, through $c = \exp - [(\Delta H^{\circ}_{ads} - \Delta H^{\circ}_{cond})/RT]$. ΔH°_{cond} is the standard enthalpy of water condensation, which is equal to -44 kJ mol^{-1} and $T = 296$ K.

the formation of metastable droplets with decreasing RH, and that water is retained by these materials at RH values below 10%.

Conclusion and atmospheric implications

Results from our studies described above have important atmospheric implications to our understanding of the aging of atmospheric HULIS due to photochemistry and role of interfacial water in their heterogeneous chemistry with gases such as NO_2. As discussed by Cwiertny *et al.*,[3] humic material is an important chromophore in aquatic systems and is involved in one of the heterogeneous photochemical pathways for HONO formation. Tannic acid was used as a model for atmospheric HULIS, and we have shown from spectroscopic studies that its photodegradation may lead to the formation of gas phase and more oxidized fragments. Our data suggests that adsorbed water is needed for the photodegradation of TA, which is consistent with the well-established efficient photodegradation of aquatic humic substances in the near UV-visible part of the electromagnetic spectrum. Although there was no enhancement in water uptake as a result of TA photodegradation under our experimental conditions, more experiments are still needed to be done at RH values higher than 30% to better understand the relationship between the extent of photodegradation and enhancement in water uptake. Resolving this issue will better our understanding of the activation of HULIS as CCN and the role of photochemistry in that process.

Moreover, our data provides evidence to the presence of more structured adsorbed water layers (or clusters) on TA that resemble interfacial water in contact with polar organic solvents. Water molecules in these layers (or clusters) have fewer hydrogen bonds than in bulk water suggesting their ability to act as hydrogen bond donors for incoming gas phase molecules. This finding might explain the activation of dried humic substances as CCN in the studies of Hatch *et al.*[10] and Chan *et al.*[9] Upon photodegradation of TA and the formation of more oxidized fragments, our data suggests further structuring in surface water. As discussed in the previous sections, such structuring reflects strong hydrogen bonding interactions between water molecules and TA, which might explain the higher content of water upon reducing RH. This observation suggests the importance to account for the adsorbed water content of atmospheric HULIS when studying their heterogeneous chemistry.

The temporal extent of the oxidative photodegradtion of TA and the existence of two kinetic regimes has important implications on our understanding of the aging process of organic-containing aerosols. The slower kinetics regime is atmospherically relevant and may describe the slow evolution of atmospheric components. While the mechanism proposed herein suggests the formation of lower molecular weight volatile organic compounds (VOCs), the chemical composition of the condensed phase changes as well due to the formation of low volatility products. This could impact the partitioning of certain gas phase molecules to the reacted solid phase. Since the slow kinetics regime is a composite of dissolution and photodegradation rates, it is important to experimentally determine the rate of formation of TA-hydrates due to gas phase water adsorption in order to accurately model the kinetics of TA oxidative photodegradation for incorporation in chemical transport models.

Our results also provide mechanistic details on the role of organic-containing aerosols in the photoenhanced reactions of gases such as NO_2. Photoenhancement of NO_2 uptake on humic acid,[12] aromatic hydrocarbons,[13,29] and pyrene[41] resulted in higher production of HONO compared to dark conditions. Photosensitised production of HONO was observed to be more under humid conditions (RH $>$ 10%), suggesting that water adsorbed on organic surfaces may play a role in this surface chemistry.[13] While there were no systematic studies that investigated the nature of water films formed on the organic surfaces in the aforementioned studies, our data suggests that water molecules strongly bind to hydrogen bond acceptors in organic materials, and hence facilitating electron transfer processes. Water films (or clusters) on organic substrates could also facilitate the formation of HONO through heterogeneous hydrolysis.[42] Clearly, carefully designed experiments are needed in this area to better understand the role of water in this photochemistry. Since the photosensitised formation of HONO accounts for 10–80% of NO_2 depending on experimental conditions, the formation of surface organonitrogen compounds is very likely and has recently been observed using ATR-FITR during the photochemical reaction of NO_2 with aromatic organic films.[29] Little is known about the formation mechanism of organonitrogen compounds in atmospheric aerosols despite the presence of alkylamines[43,44] and nitro-PAH in field-collected aerosols (see references in ref. 16). Studies on the formation of surface organonitrogen compounds from photochemical reactions of NO_2 with TA as a model for atmospheric HULIS are currently ongoing in our lab.

Acknowledgements

The authors would like to thank Dr J. Baltrusaitis in the Central Microscopy Research Facility at the University of Iowa for providing the SEM images, Drs S. Smith and S. MacNeil in the Chemistry Department at Wilfrid Laurier University for the Xe lamp and helpful discussions, respectively, and Dr C. Stroud at Environment Canada for useful comments on the manuscript. We would like to acknowledge funding from Wilfrid Laurier University, NSERC Discovery Grant, NSERC Research Tools and Instruments program, and the Canadian Foundation for Innovation-Leaders Opportunities Fund award.

References

1 Y. Rudich, N. M. Donahue and T. Mentel, *Annu. Rev. Phys. Chem.*, 2007, **58**, 321–352.
2 F. Karagulian, C. W. Dilbeck and B. J. Finlayson-Pitts, *J. Am. Chem. Soc.*, 2008, **130**, 11272–11273.
3 D. M. Cwiertny, M. A. Young and V. H. Grassian, *Annu. Rev. Phys. Chem.*, 2008, **59**, 27–51.
4 J. M. Sun and P. A. Ariya, *Atmos. Environ.*, 2006, **40**, 795–820.
5 E. R. Graber and Y. Rudich, *Atmos. Chem. Phys.*, 2006, **6**, 729–753.
6 E. Dinar, I. Taraniuk, E. R. Graber, T. Anttila, T. F. Mentel and Y. Rudich, *J. Geophys. Res., [Atmos.]*, 2007, **112**, D05211.

7 J. Sun and P. A. Ariya, *Atmos. Environ.*, 2006, **40**, 795–820.
8 K. M. Prather, C. D. Hatch and V. H. Grassian, *Annu. Rev. Anal. Chem.*, 2008, **1**, 485–514.
9 M. N. Chan and C. K. Chan, *Environ. Sci. Technol.*, 2003, **37**, 5109–5155.
10 C. D. Hatch, K. M. Gierlus, J. D. Schuttlefield and V. H. Grassian, *Atmos. Environ.*, 2008, **42**, 5672–5684.
11 M. Moonshine, Y. Rudich, S. Katsman and E. R. Graber, *Geophys. Res. Lett.*, 2008, **35**, L20807.
12 K. Stemmler, M. Ammann, C. Donders, J. Kleffmann and C. George, *Nature*, 2006, **440**, 195–198.
13 C. George, R. S. Strekowski, J. Kleffmann, K. Stemmler and M. Ammann, *Faraday Discuss.*, 2005, **130**, 195–210.
14 R. M. B. O. Duarte, E. B. H. Santos, C. A. Pio and A. C. Duarte, *Atmos. Environ.*, 2007, **41**, 8100–8113.
15 B. T. Mmereki, D. J. Donaldson, J. B. Gilman, T. L. Eliason and V. Vaida, *Atmos. Environ.*, 2004, **38**, 6091–6103.
16 S. Gross and A. K. Bertram, *J. Phys. Chem. A*, 2008, **112**, 3104–3113.
17 A. Jammoul, S. Gligorovski, C. George and B. D'Anna, *J. Phys. Chem. A*, 2008, **112**, 1268–1276.
18 C. Coury and A. M. Dillner, *Atmos. Environ.*, 2009, **43**, 940–948.
19 R. Vogt, C. Elliott, H. C. Allen, J. M. Laux, J. C. Hemminger and B. J. Finlayson-Pitts, *Atmos. Environ.*, 1996, **30**, 1729–1737.
20 J. Sirita, S. Phanichphant and F. C. Meunier, *Anal. Chem.*, 2007, **79**, 3912–3918.
21 Z. Krivacsy and J. Halvay, *Spectrochim. Acta*, 1994, **50A**, 49–55.
22 M. Jastrzebska, J. Zalewska-Rejdak, R. Wrzalik, A. Kocot, J. Mroz, B. Barwinski, A. Turek and B. Cwalina, *J. Biomed. Mater. Res., Part A*, 2006, **78a**, 148–156.
23 S. G. Moussa, T. M. McIntire, M. Szori, M. Roeselová, D. J. Tobias, R. L. Grimm, J. C. Hemminger and B. J. Finlayson-Pitts, *J. Phys. Chem. A*, 2009, **113**, 2060–2069.
24 J. J. Max and C. Chapados, *J. Phys. Chem. A*, 2007, **111**, 2679–2689.
25 J. J. Max and C. Chapados, *J. Phys. Chem. A*, 2001, **105**, 10681–10688.
26 D. B. Asay, A. L. Barnette and S. H. Kim, *J. Phys. Chem. C*, 2009, **113**, 2128–2133.
27 F. G. Moore and G. L. Richmond, *Acc. Chem. Res.*, 2008, **41**, 739–748.
28 L. F. Scatena, M. G. Brown and G. L. Richmond, *Science*, 2001, **292**, 908–912.
29 B. R. Nichols, C. Rapa, V. Costa and R. Z. Hinrichs, *J. Phys. Chem. C*, 2009, **113**, 2111–2119.
30 P. Schmitt-Kopplin, N. Hertkorn, H. R. Schulten and A. Kettrup, *Environ. Sci. Technol.*, 1998, **32**, 2531–2541.
31 Z. Droussi, V. D'Orazio, M. Hafidi and A. Ouatmane, *J. Hazard. Mater.*, 2009, **163**, 1289–1297.
32 S. I. M. Carvalho, M. Otero, A. C. Duarte and E. B. H. Santos, *Chemosphere*, 2008, **73**, 1845–1852.
33 C. Richard and S. Canonica, *in Hdb Environmental Chemistry*, Springer-Verlag, Berlin, 2005, vol. 2, pp. 299–323.
34 M. A. Young, in *Water Encyclopedia: Oceanography, Meteorology, Physics and Chemistry, Water Law, and Water History, Art, and Culture*, ed. J. Lehr and J. Kelley, Wiley & Sons, New York, 2005, pp. 529–540.
35 D. Vione, V. Maurino, C. Minero, E. Pelizzetti, M. A. J. Harrison, R.-I. Olariu and C. Arsene, *Chem. Soc. Rev.*, 2006, **35**, 441–453.
36 M. C. Gonzalez and E. S. Roman, in *Hdb Environmental Chemistry*, Springer-Verlag, Berlin, 2005, vol. 2, pp. 49–75.
37 S. A. Mang, D. K. Henricksen, A. P. Bateman, M. P. Sulbaek Andersen, D. R. Blake and S. A. Nizkorodov, *J. Phys. Chem. A*, 2008, **112**, 8337–8344.
38 A. L. Goodman, E. T. Bernard and V. H. Grassian, *J. Phys. Chem. A*, 2001, **105**, 6443–6457.
39 T. M. McIntire, A. S. Lea, D. J. Gaspar, N. Jaitly, Y. Dubowski, Q. Q. Li and B. J. Finlayson-Pitts, *Phys. Chem. Chem. Phys.*, 2005, **7**, 3605–3609.
40 M. N. Chan, S. M. Kriedenweis and C. K. Chan, *Environ. Sci. Technol.*, 2008, **42**, 3602–3608.
41 M. Brigante, D. Cazoir, B. D'Anna, C. George and D. J. Donaldson, *J. Phys. Chem. A*, 2008, **112**, 9503–9508.
42 J. Kleffmann, *ChemPhysChem*, 2007, **8**, 1137–1144.
43 K. A. Mace, N. Kubilay and R. A. Duce, *J. Geophys. Res., [Atmos.]*, 2003, **108**, 4320.
44 Q. Zhang, C. Anastasio and M. Jimemez-Cruz, *J. Geophys. Res., [Atmos.]*, 2002, **107**, 4112.
45 *CRC Handbook of Chemistry and Physics*, ed. D. R. Lide, Taylor & Francis, Boca Raton, 2006, vol. 87.
46 R. M. Silverstein and F. X. Webster, *Spectrometric Identification of Organic Compounds*, Wiley, New York, 6th edn, 1998.